Electron scattering by formamide: Elastic and electronically inelastic cross sections up to 179 energetically open states

P. A. S. Randi ⬡,[*] G. M. Moreira ⬡,[†] and M. H. F. Bettega ⬡[‡]

Departamento de Física, Universidade Federal do Paraná, Caixa Postal 19044, 81531-980 Curitiba, Paraná, Brazil

The Schwinger multichannel method with pseudopotentials was employed to obtain elastic and electronically inelastic cross sections for the scattering of electrons by formamide up to impact energies of 50 eV. The scattering calculations were carried out according to the minimal orbital basis for the single-configuration-interaction strategy and considered up to 179 open target states in the composition of the space of coupled channels for the description of the multichannel coupling. To include polarization effects, we consider only the excitations related to the hole-particle pairs used in the active space of the minimal orbital basis for the single-configuration-interaction approach. The elastic and electronically inelastic cross sections for the excitation from the ground state to the first four low-lying electronically excited states of formamide are presented, and these results are compared to previous calculations available in the literature. The partial and total ionization cross sections calculated with the binary-encounter-Bethe model and the total cross section calculated as the sum of the elastic, total electronically inelastic, and total ionization cross sections are also reported.

I. INTRODUCTION

Secondary nonthermal low-energy electrons (LEEs) produced by the interaction of high-energy radiation and matter play a significant role in the chemical reactions that occur in biological and interstellar media. In the former, LEEs are produced in vast quantities during the thermalization of the high-energy radiation used in radiotherapy and may be captured by an unoccupied molecular orbital of a biomolecule forming a transitive negative ion, also called resonance, that may lead to molecular dissociation [1]. This mechanism is called dissociative electron attachment (DEA). It was shown that it could damage genetic material through single- and double-strand breaks in DNA molecules as the LEEs are captured in the nucleotide basis [2,3], demonstrating the importance of electron-molecule interactions in the biological medium. In the interstellar medium, the interaction between high-energy ionizing cosmic radiation and matter produces a vast quantity of secondary LEEs that may play a fundamental role in the synthesis of complex organic molecules [4,5]. Therefore, to develop precise mathematical models that describe these environments, it is necessary to take into account the interaction between LEEs and molecules.

Formamide (HCONH$_2$; Fig. 1) is the simplest molecule containing a peptide bond. For this reason, it is an important building block for complex organic molecules and has been used to study low-energy electron damage on the peptide backbone of proteins [7]. Besides that, it has also been observed in the interstellar medium [8,9] and is an important prebiotic molecule that may be associated with the origin of

life itself [10]. Thus, the interactions between electrons and formamide are relevant in both the biological and interstellar environments.

Electron-formamide interactions have been studied experimentally. Seydou *et al.* [11], through electron transmission spectroscopy (ETS), reported the formation of a π^* shape resonance at 2.05 eV. Hamann *et al.* [12] studied the DEA of formamide up to 18 eV using a crossed electron-molecule beam technique and reported four resonant dissociation channels at 2.0 and 2.7 eV and between 6.0 and 7.0 eV. Li *et al.* [13], with combined experimental and computational investigations, studied in more detail the DEA mechanism of formamide. Unfortunately, to the best of our knowledge, experimental cross sections for the scattering of LEEs by formamide have not yet been reported in the literature.

On the other hand, theoretical cross sections for the scattering of electrons by formamide have been calculated, especially for impact energies below 20 eV. Bettega [14], through the Schwinger multichannel (SMC) method implemented with pseudopotentials (SMCPP), calculated the elastic integral cross sections (ICSs) and momentum-transfer cross sections (MTCSs) for the scattering of electrons by formamide in the static-exchange (SE) and static-exchange plus polarization (SEP) approximations for impact energies up to 12 eV, finding a π^* shape resonance centered around 4.5 and 2.5 eV in the SE and SEP approximations, respectively. Wang and Tian [15] calculated the elastic differential cross sections (DCSs), ICS, and MTCS as well as integral cross sections for the excitation of formamide from the ground state to its four low-lying electronically excited states using the *R*-matrix method in the SE, SEP, and close-coupling (CC) approximations for energies from 0 to 10 eV. Gupta *et al.* [16] calculated the total ionization cross section (TICS) for formamide with the spherical complex optical potential (SCOP) formalism with the complex scattering potential ion-

---
[*]pasr@fisica.ufpr.br
[†]gmm08@fisica.ufpr.br
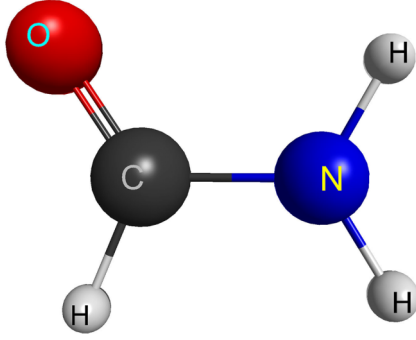[‡]bettega@fisica.ufpr.br

FIG. 1. Schematic representation of the chemical structure of formamide (generated with MACMOLPLT [6]).

ization contribution method, and the binary-encounter-Bethe (BEB) model. Homem *et al.* [17] reported elastic ICS, DCS, MTCS, total absorption cross section (TACS), and total cross section (TCS) for the scattering of electrons by formamide calculated with a single-center-expansion technique combined with the method of Padé. Vinodkumar *et al.* [18], using the *R*-matrix method in the SE, SEP, and CC approximations for the low-energy regime (below 20 eV) and the SCOP formalism for higher energies, reported elastic DCSs, the MTCS, excitation ICSs for eight electronically excited states of formamide, and the TCS. Using the SMCPP method, Silva *et al.* [19] calculated the ICS, MTCS, and DCSs for the scattering of electrons and positrons by formamide below 10 eV. More recently, the same authors investigated the role of single and double methylation on the position of the π^* shape resonance of formamide [20]. Beyond these reported cross sections, other theoretical studies have been done on the electron-formamide interactions. Goumans *et al.* [21] investigated the DEA channels of formamide, finding a π^* shape resonance around 3.77 eV and a σ^* resonance around 14.9 eV. Gallup [22] studied the shape resonances of selected organic molecules, finding a $^2A''$ resonance for formamide at 2.1226 eV.

In this work, we extend the previous results obtained with the SMCPP method [14,19,20] by including multichannel coupling effects in the scattering calculations, increasing the impact energies up to 50 eV and investigating electronically inelastic channels. Here, the ICSs and DCSs for the elastic and electronically inelastic scattering of electrons by formamide calculated with the SMCPP method with up to 179 open channels are reported. To describe the excited states we utilized the minimal orbital basis for a single configuration interaction (MOB-SCI) strategy [23]. The partial and total ionization cross sections calculated with the BEB model and the TCS are also presented. With these results, we intend to complement the set of cross sections needed to model astronomical and biological media, especially in the energy regime from 20 to 50 eV since the number of cross sections reported in the literature in this energy range is few.

The remainder of this paper is organized as follows. In Sec. II a brief discussion of the methods and the computational details used as well as the vertical excitation energies for the electronically excited states of formamide is presented. After that, in Sec. III, the results for the electron-formamide cross sections are discussed, and finally, in Sec. IV, a brief summary of our findings is given.

II. THEORY AND COMPUTATIONAL DETAILS

The Schwinger multichannel method [24] is a variational approach used to obtain the scattering amplitude. Here, we will discuss only the main aspects of this method since a more complete description can be found elsewhere [24,25]. In the present calculations we use the implementation that employs norm-conserving pseudopotentials [26] with the parameters of Bachelet *et al.* [27] to represent the nuclei and the core electrons in heavy atoms. All the calculations presented here were performed within the fixed-nuclei approximation in the optimized geometry of formamide obtained through a second order Møller-Plesset perturbation theory (MP2) with the augmented correlation-consistent polarized valence double zeta basis set (aug-cc-pVDZ) calculation with the computational package GAMESS [28] in the C_s point group.

The scattering amplitude in the SMC method is written as [25]

$$f^{\text{SMC}}(\vec{k}_f, \vec{k}_i) = -\frac{1}{2\pi} \sum_{m,n} \langle S_{\vec{k}_f} | V | \chi_m \rangle (d^{-1})_{mn} \langle \chi_n | V | S_{\vec{k}_i} \rangle, \quad (1)$$

where

$$d_{mn} = \langle \chi_m | \frac{1}{2}(PV + VP) - VG_P^{(+)}V + \frac{\hat{H}}{N+1}$$
$$- \frac{1}{2}(\hat{H}P + P\hat{H}) | \chi_n \rangle. \quad (2)$$

In the equations above, $|S_{\vec{k}_{i(f)}}\rangle$ is an eigenstate of the unperturbed Hamiltonian H_0, represented by the product of a target state and a plane wave with momentum $\vec{k}_{i(f)}$; V is the interaction potential between the incident electron and the target. $\hat{H} \equiv E - H$, where E is the collision energy and $H = H_0 + V$ is the scattering Hamiltonian. P is a projection operator onto the open-channel target space defined as

$$P = \sum_{\ell=1}^{N_{\text{open}}} |\Phi_\ell\rangle\langle\Phi_\ell|, \quad (3)$$

where $|\Phi_\ell\rangle$ is written as a single-excitation configuration-interaction wave function, N_{open} is the number of open channels, and $G_P^{(+)}$ is the free-particle Green's function projected on the P space. The $(N+1)$-electron trial configuration-state functions (CSFs) $\{|\chi_m\rangle\}$ are given as products of target states with single-particle scattering orbitals with the proper spin coupling,

$$|\chi_{mn}\rangle = \mathcal{A}|\Phi_m^s\rangle \otimes |\varphi_n\rangle, \quad (4)$$

where $\mathcal{A}$ is an antisymmetrization operator and $|\Phi_m^s\rangle$ is a state of the molecule, where $m = 0$ corresponds to the ground state and $m > 0$ corresponds to a singly electronically excited state that represents the promotion of an electron from a hole (occupied) orbital to a particle (unoccupied) orbital with singlet ($s = 0$) or triplet ($s = 1$) spin coupling.

All the valence electrons of the formamide molecule were represented using Cartesian Gaussian functions. For the carbon, oxygen, and nitrogen atoms the valence electrons

TABLE I. Exponents of the uncontracted basis functions for the C, N, and O atoms.

Type	C	N	O
s	12.49628	17.56734	16.05878
s	2.470286	3.423615	5.920242
s	0.614028	0.884301	1.034907
s	0.184028	0.259045	0.316843
s	0.039982	0.055708	0.065203
s	0.009996	0.013927	0.016301
p	5.228869	7.050692	10.14127
p	1.592058	1.910543	2.783023
p	0.568612	0.579261	0.841010
p	0.210326	0.165395	0.232940
p	0.072250	0.037192	0.052211
d	1.794795	0.975569	1.698024
d	0.420257	0.253058	0.455259
d	0.101114	0.078904	0.146894

were described by the $6s5p3d$ basis set with the exponents listed in Table I and were generated according to [29]. To describe the hydrogen atoms we employed the $4s/3s$ basis set of Dunning [30] increased by one p-type function with the exponent equal to 0.75.

Through the use of the improved virtual orbitals [31] generated from the highest occupied orbital of a' symmetry, we ran a full single configuration interaction (FSCI) calculation, and then a minimal orbital basis for a single-configuration-interaction approach [23] was constructed. In this work, the electronically excited states obtained from the MOB-SCI calculation were constructed with 89 hole-particle pairs. This procedure was able to reproduce the lowest 20 states obtained with FSCI calculations. To assess the quality of the electronically excited states obtained with these single-configuration-interaction techniques a more robust electronic-structure calculation with the equation-of-motion coupled-cluster with singles and doubles (EOM-CCSD) [32–35] method and the

augmented correlation-consistent polarized valence double zeta (aug-cc-pVDZ) basis set was performed using the computational package PSI4 [36]. In Table II, these results are summarized and compared to theoretical [15,18,37,38] and experimental [39–41] results found in the literature. The results of the MOB-SCI reproduce well those calculated via the FSCI. Although an overall satisfactory agreement with the results from the literature is found [15,18,37–41], these single-configuration-interaction approaches have two shortcomings: the first one is that the order of the two lowest electronically excited states ($1^3A'$ and $1^3A''$) is inverted in relation to more robust electronic-structure calculations. The second one is that the electronically excited states of A' symmetry are not well described. A schematic representation of the MOB-SCI spectrum is presented in Fig. 2. Following this procedure, our scattering calculations were performed at a level up to 179 channels treated as open (89 singlets + 89 triplets + ground state).

The same 89 hole-particle pairs used for the MOB-SCI construction were employed in the scattering calculations to obtain the set of determinants $|\Phi_m\rangle$ included in the construction of the CSFs [see Eq. (4)], and all unoccupied molecular orbitals were used as scattering orbitals. With this procedure, we obtained 5554 CSFs of A' symmetry and 5786 of A'' symmetry. The number of A'' CSFs is comparable to the ones used in previous calculations performed with the SMCPP method that aimed to describe the low-energy electron-formamide scattering [14,19]. Therefore, we expect that the polarization effects of the target due to the incident electron are well described by this configuration space. This expectation is indeed correct since the position of the π^* shape resonance agrees well with the data presented in the literature, as will be discussed in Sec. III. The components of the spherical polarizability of formamide are $\alpha_{xx} = 20.15$ au, $\alpha_{yy} = 28.79$ au, and $\alpha_{zz} = 34.46$ au [42].

The scattering calculations were performed with different levels of multichannel coupling; that is, a different number of electronically excited states were included in the construction of the projector operator given in Eq. (3). In order to

TABLE II. Vertical excitation energies (in eV) for the first 10 excited electronic states obtained from FSCI, MOB-SCI, and EOM-CCSD/aug-cc-pVDZ calculations. We compared our results with the theoretical results of Wang and Tian complete active space configuration interaction with the correlation-consistent polarized valence triple zeta basis set (CAS-CI/cc-pVTZ) [15], Vinodkumar *et al.* configuration interaction with the Pople 6-311G basis set (CI/6-311G) [18], Chong time dependent density functional theory with the statistical average of orbital potentials and the even-tempered polarized valence quadruple zeta basis set [TDDFT/(SAOP)/et-pVQZ] [37], and Hirst *et al.* (MRCI/6-31+g**) and also with the experimental results of Gingell *et al.* [vacuum ultraviolet (VUV) and electron-energy-loss spectroscopy] [39], Staley *et al.* (ion cyclotron resonance detection) [40], and Basch *et al.* (VUV) [41].

| State	FSCI	MOB-SCI	EOM-CCSD	Ref. [15]	Ref. [18]	Ref. [37]	Ref. [38]	Expt.
$1^3A'$	5.368	5.572	5.605	5.24		5.64		6.0 [39]
$1^3A''$	5.675	5.841	5.238	5.71	6.07	5.23		5.2 [39], 5.30 [40]
$1^1A''$	6.331	6.416	5.572	5.49		5.71	5.86	5.82 [39], 5.65 [41]
$2^3A''$	7.259	7.450	6.481	6.30				
$2^1A''$	7.646	7.745	6.694	6.72	6.47	7.32	6.14	
$2^1A'$	8.378	8.644	6.795	6.95		6.64	6.49	6.35 [39], 6.80 [41]
$3^3A''$	8.440	8.546	7.482	7.62			7.01	
$2^3A'$	8.510	8.609	6.731	6.98	6.63	6.48		6.4 [39]
$3^1A''$	8.593	8.651	7.546	7.77		8.07		
$3^3A'$	8.624	8.930	7.306	7.63	8.91			
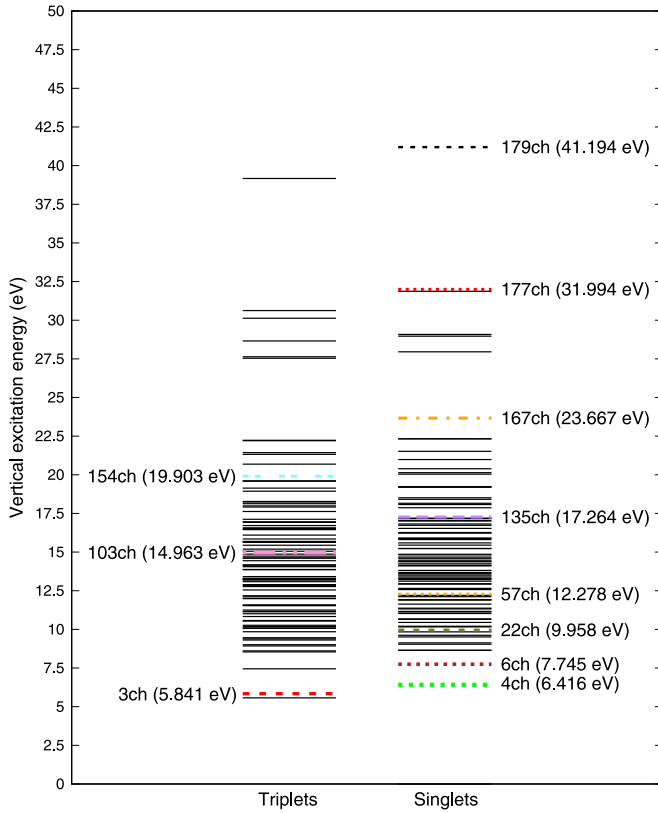
FIG. 2. Schematic representation of the vertical excitation energies (in eV) of the 178 electronically excited states of formamide obtained with the MOB-SCI calculation and the different multichannel coupling strategies employed in the scattering calculations. The dashed red line corresponds to the threshold of the 3ch scattering calculation; dotted green line, 4ch; dotted brown line, 6ch; dashed olive line, 22ch; dotted orange line, 57ch; dash-double-dotted pink line, 103ch; dashed purple line, 135ch; double-dashed cyan line, 154ch; dash-dotted orange line, 167ch; dotted red line, 177ch. The 179ch threshold is also indicated.

distinguish the different levels of channel coupling considered in our calculations, we used terminology already used in other works (see, for instance, [43]), N_{open}ch, where N_{open} is the number of channels treated as open in that level of approximation. Concerning the coupling level, the scattering calculations were performed following the strategy 3ch, 4ch, 6ch, 22ch, 57ch, 103ch, 135ch, 154ch, 167ch, 177ch, and 179ch, where the thresholds of each level of calculation are presented in Fig. 2. It is important to note that even if a specific channel is not treated as open in a particular level of calculation, it is still included in the configurational space as a closed channel. As a consequence, these closed channels contribute to the correlation of the scattering wave function and to the description of the polarization effects of the molecular target. On the other hand, the ICS calculated with fewer open channels presents pseudoresonances in the high-energy regime (as will be shown in the next section). These structures have no physical meaning and are a result of channels that are energetically accessible but treated as closed in these levels of calculation. These pseudoresonances are expected to disappear if all energetically accessible channels are treated as open in each impact energy. Although

TABLE III. Chosen values for ℓ_{SMC} for the Born-closure procedure performed in the calculations of the elastic cross sections. Energy ranges are presented in eV.

ℓ_{SMC}	Energies	ℓ_{SMC}	Energies
1	1.0 to 1.9	6	25.0 to 30.0
2	2.0 to 3.5	7	31.0 to 44.0
3	4.0 to 6.5	8	45.0
4	6.6 to 12.0	9	46.0 to 50.0
5	12.5 to 24.0		

this would be the ideal case, it is currently computationally impossible to perform for every impact energy since for each level of calculation a different projector operator [Eq. (3)] has to be constructed, and thus, 179 distinct scattering calculations with a fine energy grid would have to be performed.

The formamide molecule has a permanent dipole moment of 4.35 D obtained in our calculations, which overestimates the experimental value of 3.73 D [44]. In the SMC method square integrable (L^2) functions are used for the expansion of the scattering wave function, which truncates the long-range dipole interaction. In order to include the description of long-range effects on cross sections we used the Born-closure procedure following the same strategy described in Ref. [25]. The scattering amplitude obtained with the Born-closure procedure is written as

$$f(\vec{k}_f, \vec{k}_i) = f^{FBA}(\vec{k}_f, \vec{k}_i) + \sum_{\ell=0}^{\ell_{SMC}} \sum_{m=-\ell}^{\ell} \left[f_{\ell m}^{SMC}(k_f, \vec{k}_i) - f_{\ell m}^{FBA}(k_f, \vec{k}_i) \right] Y_{\ell m}^*(\hat{k}_f), \quad (5)$$

where f^{FBA} corresponds to the scattering amplitude obtained from the first Born approximation (FBA). Both $f_{\ell m}^{FBA}$ and $f_{\ell m}^{SMC}$ are obtained through expansion of FBA and SMC scattering amplitudes in terms of spherical harmonics. The SMC method accurately describes the short-range interaction between the incident electron and the target molecule. Thus, for partial waves with small angular momentum ($\ell < \ell_{SMC}$) the SMC results are used. On the other hand, the SMC is not suitable for higher partial waves ($\ell > \ell_{SMC}$) since the long-range dipole interaction is poorly described. Therefore, for higher values of ℓ we use the partial waves acquired for the dipole potential from FBA. We choose the ℓ_{SMC} that presents good agreement between the differential cross sections calculated utilizing the Born closure and the SMC method at high scattering angles. The ℓ_{SMC} used in each energy regime are listed in Table III.

To obtain the total cross section it is necessary to calculate, in addition to the elastic and electronically inelastic cross sections, the ionization cross section. As the SMC method does not take into account the ionization channel, it is necessary to estimate it, and for this purpose, we use the BEB model [45]. The total ionization cross section is obtained as

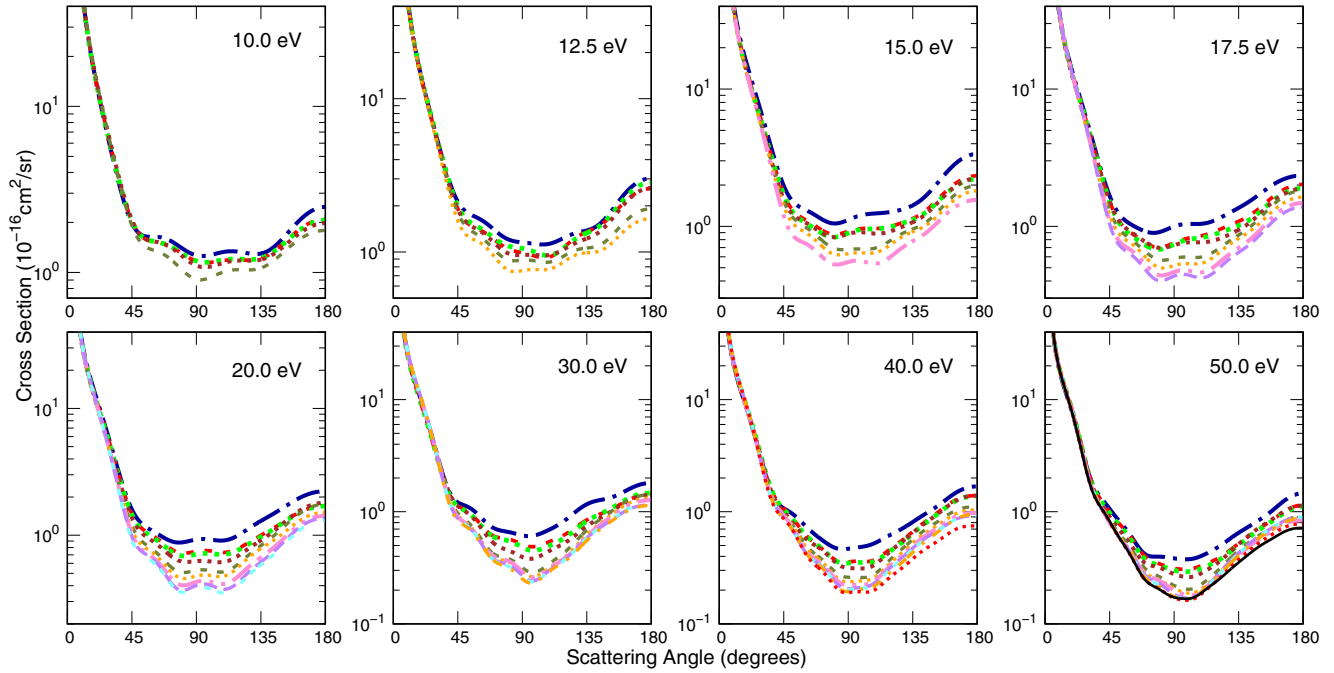$$\sigma_{BEB} = \sum_{i=1}^{N_{occ}} \sigma_i(t_i), \quad (6)$$

FIG. 3. Elastic differential cross section for the scattering of electrons by formamide calculated with different multichannel coupling schemes at 10, 12.5, 15, 17.5, 20, 30, 40, and 50 eV. Long-dash-dotted blue line, 1ch; dashed red line, 3ch; dotted green line, 4ch; dotted brown line, 6ch; dashed olive line, 22ch; dotted orange line, 57ch; dash-double-dotted pink line, 103ch; dashed purple line, 135ch; double-dashed cyan line, 154ch; dotted orange line, 167ch; dotted red line, 177ch; and solid black line, 179ch. The long-range dipole interaction between the incident electron and the molecule and the multichannel coupling effects are observed.

where N_{occ} is the number of occupied molecular orbitals of the target and σ_i is given by the expression

$$\sigma_i(t_i) = \frac{4\pi a_0^2 N_i (R/B_i)^2}{t_i + u_i + 1} \left[\frac{\ln(t_i)}{2} \left(1 - \frac{1}{t_i^2} \right) + 1 - \frac{1}{t_i} - \frac{\ln(t_i)}{t_i + 1} \right],$$

(7)

where a_0 is the Bohr radius, N_i is the occupation number of the ionizing orbital, R is the Rydberg energy, and B_i is the bound-state biding energy of the ionizing orbital. $t_i = E/B_i$, and $u_i = U_i/B_i$, where E is the electron incident energy and U_i is the orbitals' average kinetic energy. The necessary parameters for this calculation were obtained in the equilibrium ground-state geometry at the Hartree-Fock calculation performed with the aug-cc-pVDZ basis set as implemented in the GAMESS computational package [28]. This calculation indicates that the ionization threshold for formamide is 11.527 eV, in good agreement with the calculation performed by Vinodkumar *et al.* [18] and overestimating the experimentally determined adiabatic and vertical ionization energies of 10.23 eV [46,47] and 10.42 eV [47], respectively.

III. RESULTS AND DISCUSSION

In this section the results for the elastic, electronically inelastic, ionization, and total cross sections will be discussed.
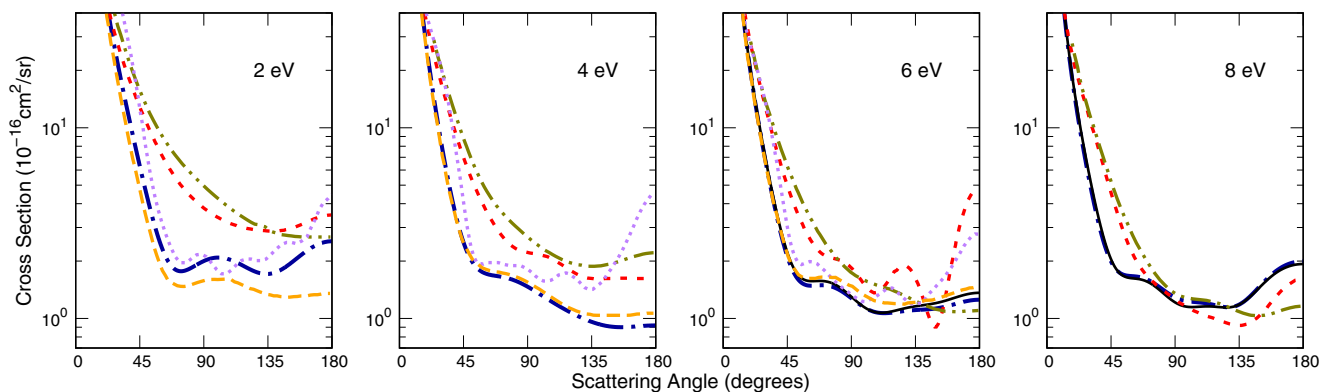

FIG. 4. Elastic differential cross sections for impact energies of 2, 4, 6, and 8 eV. Dash-dotted blue line, present 1ch; solid black line, present calculation with the best multichannel coupling scheme (3ch at 6 eV and 6ch at 8 eV); short-dashed red line, Ref. [15]; dotted purple line, Ref. [17]; dash-double-dotted olive line, Ref. [18]; dashed orange line, Ref. [19].

For better organization of these results, we present them in different subsections.

A. Elastic channel

The elastic DCSs calculated with the SMCPP with different multichannel coupling schemes are presented in Fig. 3 for impact energies of 10, 12.5, 15, 17.5, 20, 30, 40, and 50 eV. The Born-closure procedure was performed for these DCSs. The multichannel coupling effect can be observed; that is, the magnitude of the elastic DCSs decreases as the number of open channels increases in the scattering calculations. This occurs because the electronically inelastic channels compete for the flux that defines the elastic cross section, lowering its magnitude. A useful analogy to understand this effect is that of a water dam [48]: imagine that, initially, only one gate is open; then all the water will flow only through this gate. If more gates are opened, the flow of water will be shared with these other gates, lowering the flux that passes through the original gate. In the case of the electron-formamide scattering the 1ch calculation has only the elastic channel treated as open, and as a consequence, the whole flux defines only the elastic cross section. As the molecule is allowed to be electronically excited ($N_{open} > 1$), the magnitude of the elastic DCS decreases because the now opened inelastic channels compete for part of the flux that before defined only the elastic cross section. This multichannel coupling effect becomes more relevant at higher impact energies since more channels are energetically accessible. Apart from that, since formamide is a polar molecule we also observe a high forward scattering at all impact energies for all multichannel coupling schemes as a consequence of the long-range dipole interactions between the electron and molecular target.

In Figs. 4 and 5 we present the elastic DCSs calculated with only the elastic channel open (1ch) and with the best multichannel coupling scheme for each energy (3ch at 6 eV, 6ch at 8 eV, 22ch at 10 and 12 eV, and 57ch at 14 eV) along with the results from the literature [15,17–19]. The 1ch calculation agrees well with the previous results of Silva *et al.* [19] that were obtained with the SMCPP method, as expected. The only exception is at 2 eV, where the position of the shape resonance in the elastic ICS (which will be shown later in this section) is responsible for the differences between the present results and the ones reported by Silva *et al.* [19]. The comparison between the present elastic DCSs and the ones from the literature calculated with other methods [15,17,18] is poor. At 2 and 4 eV the DCSs disagree in both the overall magnitude and the oscillatory behavior. Once again, these differences may be an effect of the positioning of the shape resonance in the ICS due to the different polarization schemes used in these calculations. At 6, 8, 10, 12, and 14 eV the overall magnitude of all the calculated DCSs are similar, but the oscillatory behavior differs. Unfortunately, the lack of experimental data makes it impossible to scrutinize these differences in the theoretical DCSs beyond conjectures.

The elastic ICSs calculated without the Born-closure procedure with different multichannel coupling schemes are presented in Fig. 6. A shape resonance centered at 2.18 eV is seen in our 1ch ICS. As is the case for the DCSs shown in Fig. 3, the multichannel coupling effect is observed: the
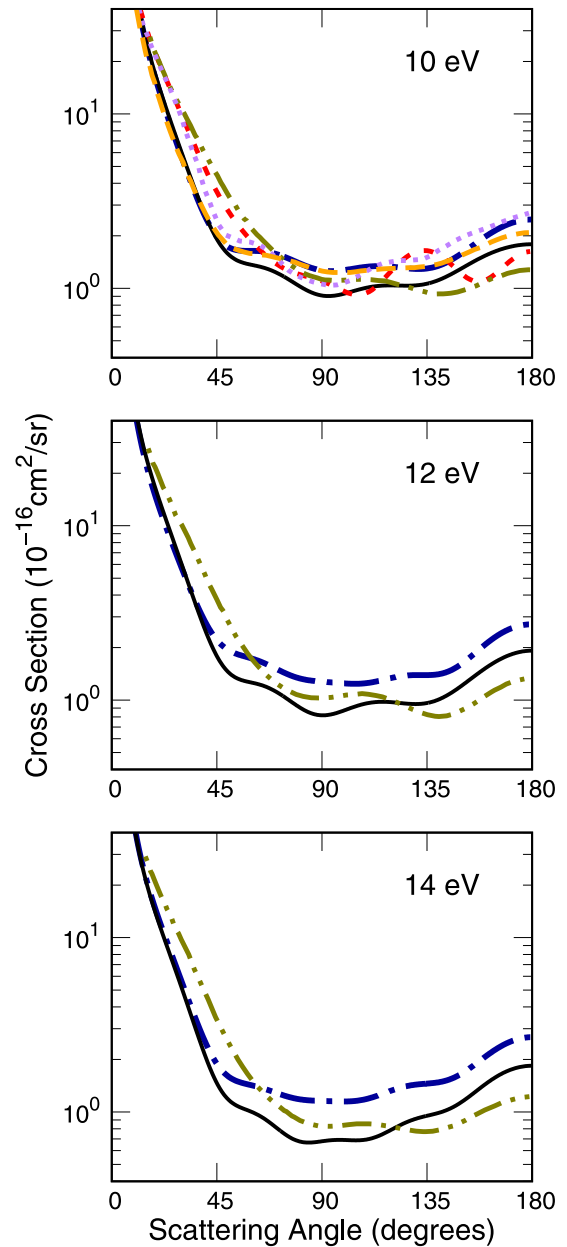

FIG. 5. Elastic differential cross sections for impact energies of 10, 12, and 14 eV. Dash-dotted blue line, present 1ch; solid black line, present calculation with the best multichannel coupling scheme (22ch at 10 and 12 eV and 57ch at 14 eV); short-dashed red line, Ref. [15]; dotted purple line, Ref. [17]; dash-double-dotted olive line, Ref. [18]; dashed orange line, Ref. [19].

magnitude of the ICS decreases as more channels are treated as open in the scattering calculations. In the 1ch calculation, pseudoresonances are present in the ICS for impact energies above the first excitation threshold (5.572 eV). These structures are a consequence of energetically accessible channels that are treated as closed in this level of approximation. In the calculations where more channels are treated as open, these pseudoresonances tend to vanish from the ICS, up to a point where all electronically inelastic channels are treated as open (179ch) and the cross section is structureless. This
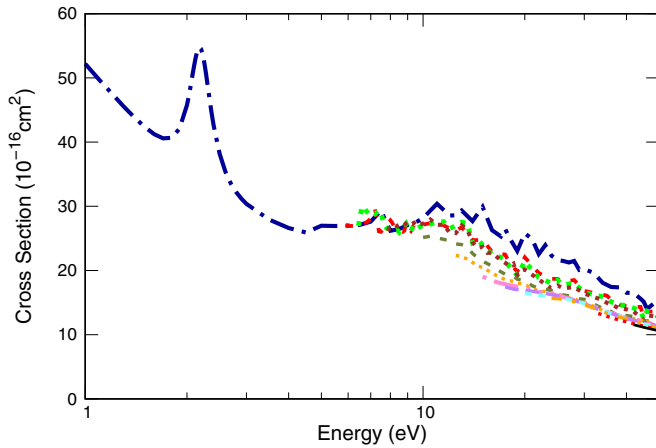
FIG. 6. Elastic integral cross section calculated with different multichannel coupling schemes without the Born-closure procedure. Dash-dotted blue line, 1ch; dashed red line, 3ch; dotted green line, 4ch; dotted brown line, 6ch; dashed olive line, 22ch; dotted orange line, 57ch; dash-double-dotted pink line, 103ch; dashed purple line, 135ch; double-dashed cyan line, 154ch; dotted orange line, 167ch; dotted red line, 177ch; and solid black line, 179ch.

is expected and is a well-known characteristic of the SMCPP method.

The calculated elastic ICSs with the best multichannel coupling scheme for each energy regime, that is, 1ch up to 5.841 eV, 3ch from 5.841 to 6.416 eV, 4ch from 6.416 to 7.745 eV, 6ch from 7.745 to 9.958 eV, 22ch from 9.958 to 12.278 eV, 57ch from 12.278 to 14.963 eV, 103ch from 14.963 to 17.264 eV, 135ch from 17.264 to 19.903 eV, 154ch from 19.903 to 23.667 eV, 167ch from 23.667 to 31.994 eV, 177ch from 31.994 to 41.194 eV, and 179ch for energies above 41.194 eV, with the Born-closure procedure and the results from the literature are presented in Fig. 7. As opposed to the elastic DCSs, which give a more detailed description of the scattering process, the differences in the calculations performed here and in previous works are averaged out in the ICS, and overall good agreement is found. In the present
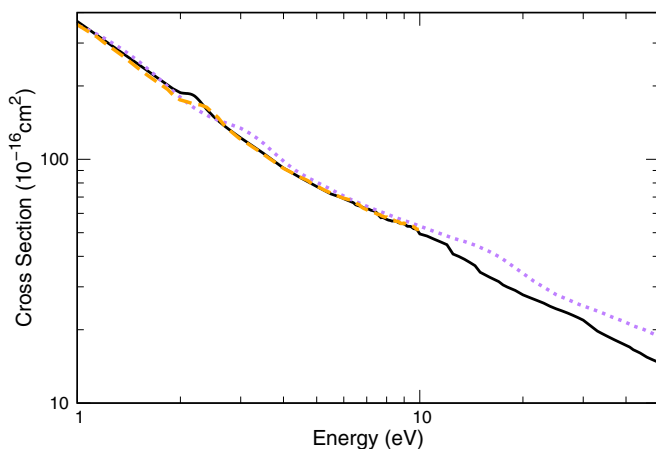

FIG. 7. Integral elastic cross section calculated employing the Born-closure procedure. Solid black line, present ICS; dashed purple line, ICS from Ref. [17]; dashed orange line, SEP ICS from Ref. [19].

TABLE IV. Position of the shape resonance found by the present calculation and from the literature (in eV).

Reference	Energy
Present study	2.18
Seydou *et al.* [11]	2.05
Hamann *et al.* [12]	2.0–2.7
Bettega [14]	2.5
Wang and Tian [15]	2.25 (SEP), 2.67 (CC)
Homem *et al.* [17]	3.5
Vinodkumar *et al.* [18]	3.41
Silva *et al.* [19]	2.38
Silva *et al.* [20]	2.32 (SEP1), 2.46 (SEP3)
Goumans *et al.* [21]	3.77
Gallup [22]	2.1226

calculation the well-known π^* shape resonance is centered at 2.18 eV, which is in good agreement with the result from Seydou *et al.* [11], Hamann *et al.* [12], Bettega [14], the SEP results from Wang and Tian [15], both works from Silva *et al.* [19,20], and Gallup [22] but underestimates the results from Wang and Tian [15] in the CC approximation and the ones from Homem *et al.* [17], Vinodkumar *et al.* [18], and Goumans *et al.* [21]. A comparison of the position of the shape resonance found by us in the present work and the ones mentioned from the literature is given in Table IV. It is worth noting that in the present calculation there is a tail of the π^* shape resonance at 2 eV, while in the ICS from Silva *et al.* [19] the resonance is centered at slightly higher energy, which explains the differences found in the elastic DCS at 2 eV (Fig. 4). Beyond that, in the energy regime from 6 to 20 eV the spectrum of electronically excited states of formamide is the densest, as can be seen from Fig. 2. As a consequence, a high number of channels are treated as closed even in the best multichannel coupling schemes used in our calculations in this energy regime, and pseudoresonances appear in the ICS. Also, a distinct shape resonance around 15 eV does not appear in the calculated ICS, in contrast to the studies performed by Goumans *et al.* [21], Homem *et al.* [17], and Vinodkumar *et al.* [18]. This resonance may be hidden by the pseudoresonances present in the ICS.

B. Electronic excitation channel

The DCSs for the electronic excitation from the ground state to the $1^3A'$ (5.572 eV), $1^3A''$ (5.841 eV), $1^1A''$ (6.416 eV), and $2^3A''$ (7.450 eV) states of formamide for selected energies are presented in Figs. 8–11, respectively. The cross sections are mostly isotropic, and the multichannel coupling effect is observed. The magnitude of the DCSs does not decreases uniformly as the number of open channels increases in the scattering calculation; that is, the low-lying electronically excited states tend to compete more actively for the flux that defines the cross section than the higher-lying states. This can be seen in our results when we compare the DCSs calculated with up to the 103 open channels, where the difference in magnitude is noticeable; meanwhile, the magnitudes of the DCSs calculated with higher channel coupling schemes ($N_{\text{open}} > 103$) are similar.
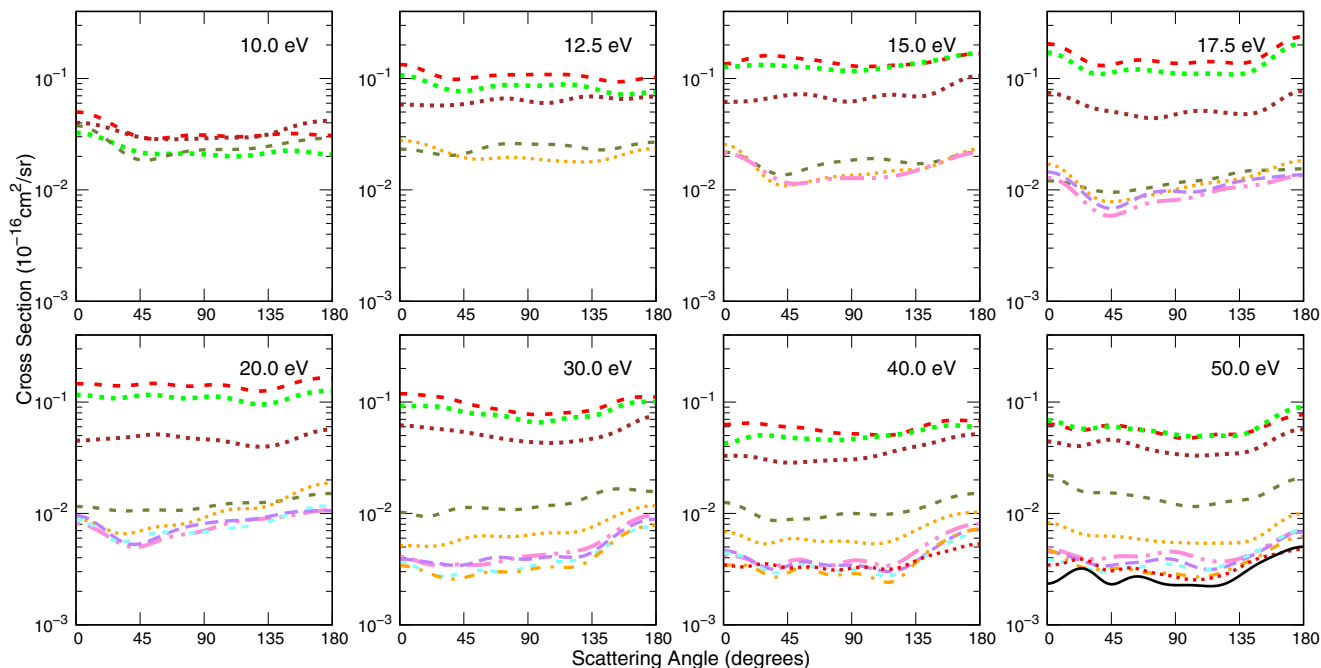
FIG. 8. Differential cross sections for the electronic excitation of the $1^3A'$ (5.572 eV) state of formamide for impact energies of 10, 12.5, 15, 17.5, 20, 30, 40, and 50 eV. Dashed red line, 3ch; dotted green line, 4ch; dotted brown line, 6ch; dashed olive line, 22ch; dotted orange line, 57ch; dash-double-dotted pink line, 103ch; dashed purple line, 135ch; double-dashed cyan line, 154ch; dot-dashed orange line, 167ch; dotted red line, 177ch; solid black line, 179ch.

It is worth noting that in some cases the DCSs calculated with fewer open channels have a lower magnitude than the ones calculated with a larger open channel space. These inversions are a result of pseudoresonances in the calculations with fewer open channels. Also, the electronic excitation from the ground state to $1^1A''$ (6.416 eV) is dipole allowed, and as a

consequence, long-range interactions play a significant role in the scattering process. Here, the Born-closure procedure was not performed, and we expect the DCSs reported in Fig. 10 to be underestimated for low scattering angles (below 20°).

The ICSs for the electronic excitation from the ground state to the $1^3A'$ (5.572 eV), $1^3A''$ (5.841 eV), $1^1A''$ (6.416 eV), and
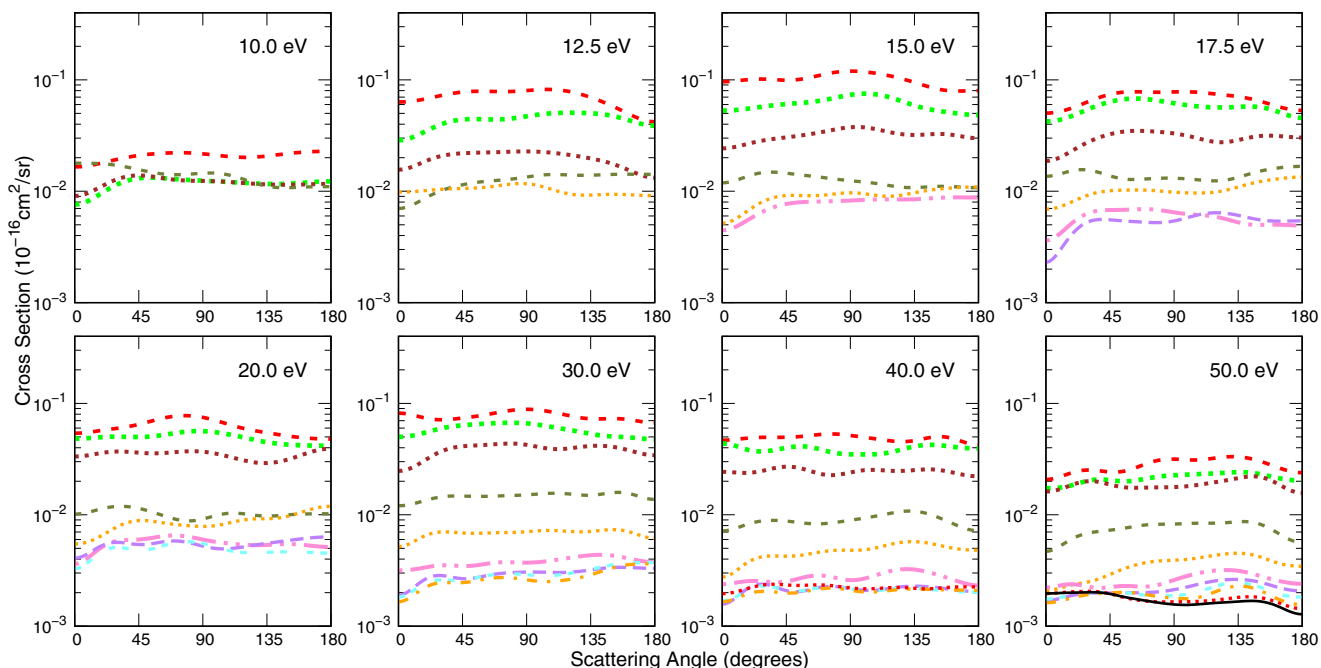

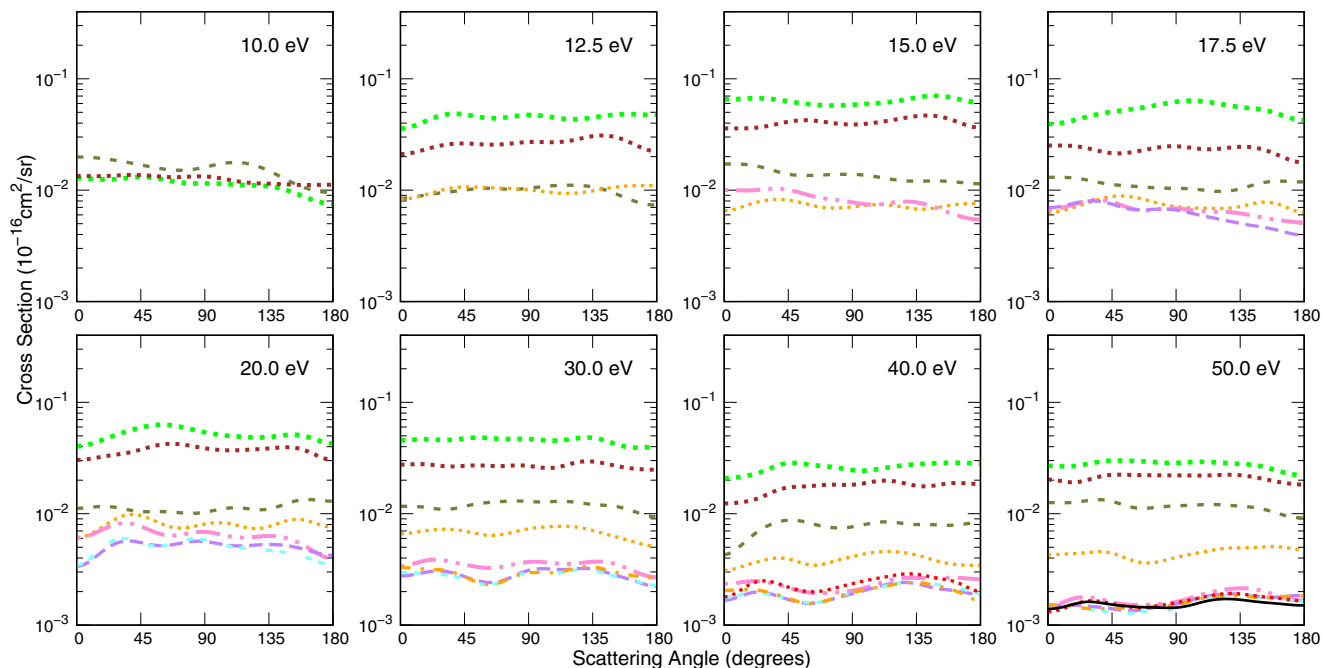FIG. 9. Same as Figure 8, but for the $1^3A''$ (5.841 eV) state.

FIG. 10. Same as Figure 8, but for the $1^1A''$ (6.416 eV) state.

$2^3A''$ (7.450 eV) states of formamide are presented in Fig. 12, along with the results of Wang and Tian [15] and Vinodkumar *et al.* [18]. The best multichannel coupling scheme was used in each energy regime. As is the case of the elastic ICS, the cross sections calculated here present a high number of pseudoresonances for impact energies from 6 to 20 eV as a consequence of the high density of electronically excited states of formamide (and of closed channels that are energetically accessible) in this energy regime. At impact energies above 20 eV the calculated cross sections are structureless

since the spectrum of electronically excited states obtained within the MOB-SCI approach at these energies is less dense and more channels are treated as open in the scattering calculations.

The comparison between the present electronically inelastic ICS and the results found in the literature is poor. Since our calculations present a high density of electronically excited states between 6 and 20 eV, we cannot distinguish core-excited and Feshbach resonances from pseudoresonances. Another calculation performed with a less dense spectrum
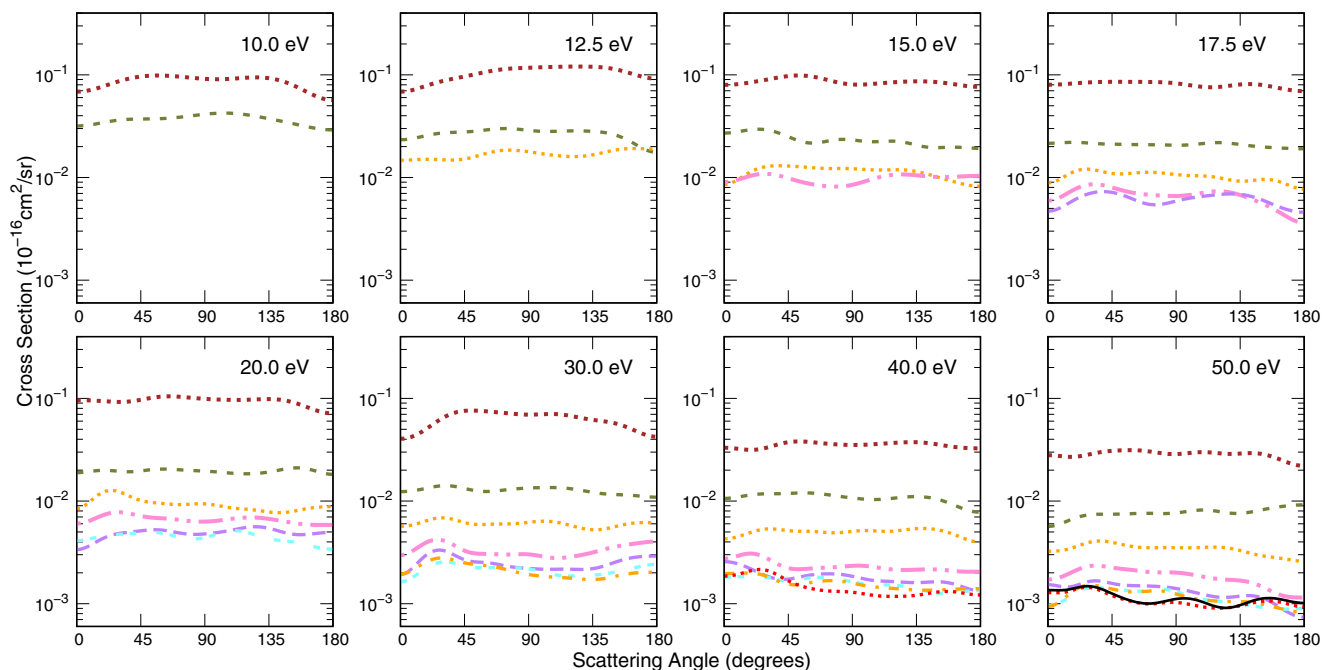

FIG. 11. Same as Figure 8, but for the $2^3A''$ (7.450 eV) state.
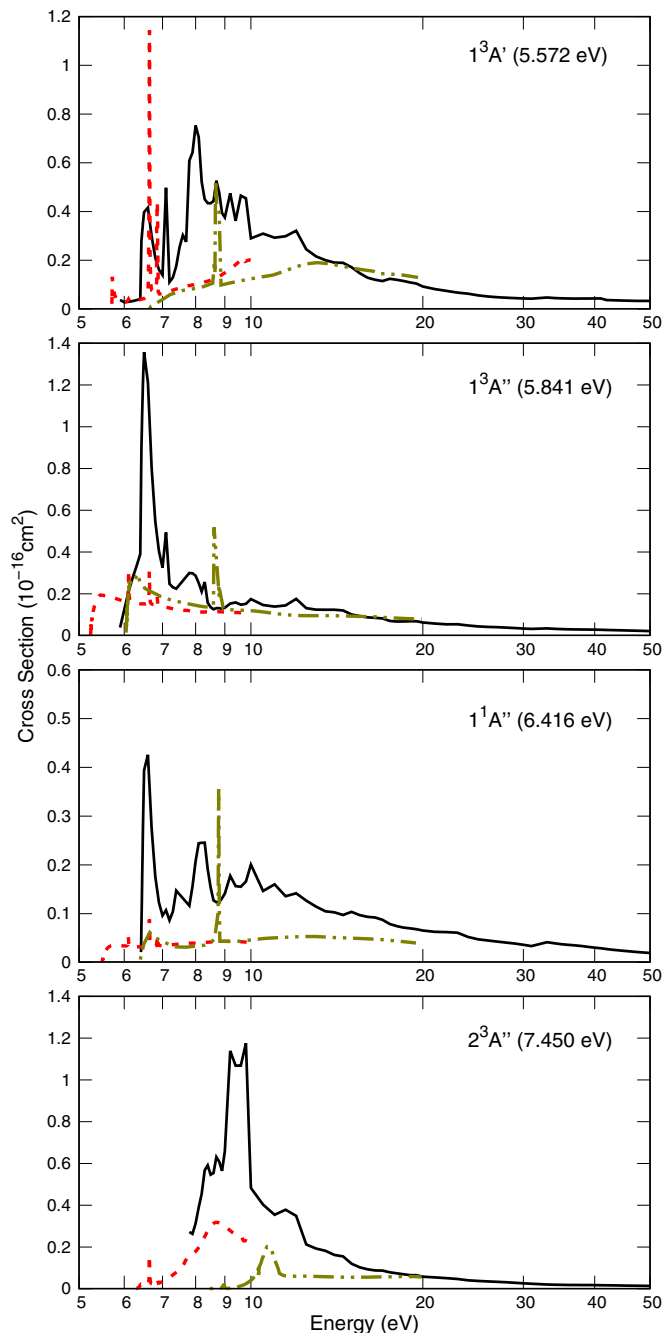
FIG. 12. Integral cross sections for the excitation from the ground state to the $1^3A'$ (5.572 eV), $1^3A''$ (5.841 eV), $1^1A''$ (6.416 eV), and $2^3A''$ (7.450 eV) states of formamide. Solid black line, present ICS; dashed red line, Ref. [15]; dash-double-dotted olive line, Ref. [18].

in this energy regime would be necessary to make this distinction, but it is beyond the scope of this work since our primary goal is to study the electron scattering at intermediate impact energies (20 to 50 eV). Nevertheless, note that although performed with the same method, the two *R*-matrix results from the literature do not agree in regards to the number, position, and character of the resonances found in the electronically inelastic cross section. Wang and Tian [15] found three Feshbach shape resonances and
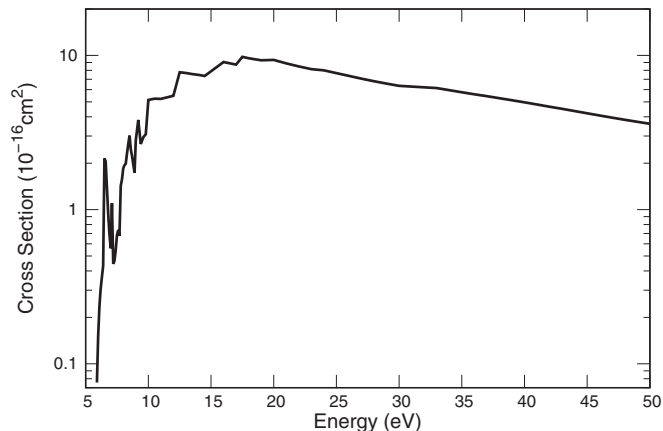

FIG. 13. Total excitation cross section calculated as the sum of all electronically inelastic cross sections. The structures below 20 eV are pseudoresonances associated with closed channels in the scattering calculation, while the cross section is smooth for higher impact energies.

one mixed core-excited shape resonance, while Vinodkumar *et al.* [18] found two Feshbach and three mixed core-excited shape resonances. This emphasizes the challenges of dealing with an electronically inelastic scattering calculation from the theoretical point of view, where the cross sections and resonances are extremely sensitive to the description of the electronically excited states and to the multichannel coupling treatment.

To further enhance the data set regarding the electronic excitation of formamide, the total excitation cross sections (TECSs) calculated as the sum of all electronically inelastic ICSs are presented in Fig. 13. Once again, pseudoresonances can be observed for impact energies below 20 eV, while the cross section is smooth for higher impact energies.

C. Ionization cross section

The electronic configuration of the ground state of formamide is $(1a')^2(2a')^2(3a')^2(4a')^2(5a')^2$ $(6a')^2(7a')^2(8a')^2(9a')^2(1a'')^2(10a')^2(2a'')^2$. The partial ionization cross sections for each of these molecular orbitals calculated with the BEB/aug-cc-pVDZ model are presented in the top panel of Fig. 14. The core molecular orbitals, namely, $(1a')^2(2a')^2(3a')^2$, have a high ionization potential (309.18, 424.51, and 558.91 eV, respectively), and as a consequence, their ionization cross sections do not contribute considerably in this energy regime.

The TICS calculated as the sum of the partial ionization cross sections of each molecular orbital, the TICS from Gupta *et al.* [16], and the TACS from Homem *et al.* [17] are presented in the bottom panel of Fig. 14. The present TICS has a maximum at 91 eV and agrees well with the results of Gallup [22], underestimating the results from Homem *et al.* [17]. This is expected since the TACS involves channels beyond the single ionization channel. Note that this channel does not compete for the flux that defines the cross sections calculated with the SMC method. This is a separate calculation to estimate the TICS.
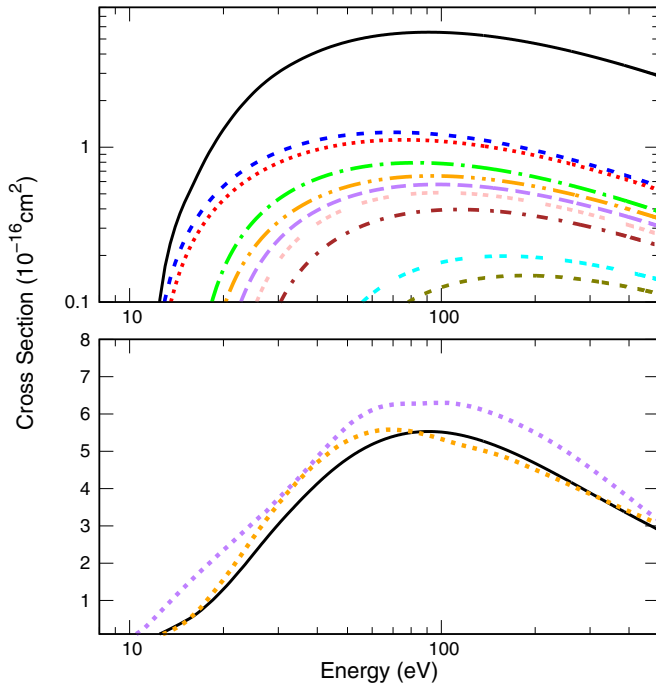
FIG. 14. Ionization cross sections for formamide. Top: partial ionization cross section for the $(2a'')^2$ molecular orbital, dashed blue line; $(10a')^2$, short-dashed red line; $(1a'')^2$, dash-dotted green line; $(9a')^2$, dash-double-dotted orange line; $(8a')^2$, dashed purple line; $(7a')^2$, triple-dashed pink line; $(6a')^2$, short-dashed brown line; $(5a')^2$, double-dashed cyan line; and $(4a')^2$, dashed olive line. The total ionization cross section is also presented as the solid black line. Bottom: solid black line, present TICS; dashed orange line, TICS from Ref. [16]; dashed purple line, TACS from Ref. [17].

D. Total cross section

The TCS was calculated as the sum of the elastic ICS (Fig. 7), the TECS (Fig. 13), and the BEB TICS (Fig. 14). It is presented in Fig. 15 along with TCSs reported in the literature [17,18]. The TCS presents the well-known π^* reso-
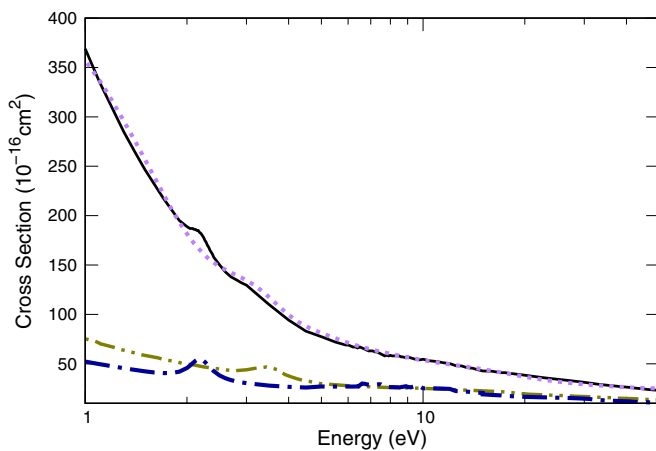

FIG. 15. Total cross section for the scattering of electrons by formamide. Solid black line, present TCS; dashed purple line, TCS from Ref. [17]; dash-double-dotted olive line, TCS from Ref. [18]; dash-dotted blue line, elastic ICS calculated without the Born-closure procedure.

TABLE V. Magnitude (in Å^2) of the elastic ICS, TECS, TICS, and TCS at 20, 25, 30, 35, 40, 45, and 50 eV.

Energy	ICS	TECS	TICS	TCS
20	27.80	9.34	1.30	38.44
25	24.37	7.68	2.25	34.30
30	21.88	6.35	3.04	31.27
35	18.90	5.77	3.65	28.32
40	17.26	4.96	4.13	26.35
45	15.73	4.21	4.51	24.45
50	14.65	3.60	4.80	23.05

nance centered at 2.18 eV and high magnitude for low impact energies associated with the long-range dipole interactions between the incident electron and the molecule. Good agreement with the results from Homem *et al.* [17] is found, while the present TCS overestimates the one reported by Vinodkumar *et al.* [18]. We also point out that although Vinodkumar *et al.* [18] performed the Born-closure procedure in their calculations, the TCS reported by these authors is close in magnitude to the elastic ICS calculated without the Born-closure procedure in the present work. Finally, the explicit numerical values of the elastic ICS (calculated using the SMC method with the Born-Closure procedure), the TECS, the TICS, and the TCS for selected impact energies where our calculations are most stable (20 to 50 eV) are presented in Table V.

IV. CONCLUSION

The elastic and electronically inelastic ICS and DCSs for the scattering of electrons by formamide were calculated with the SMCPP method within the MOB-SCI approach with up to 179 channels treated as open in the scattering calculations. The multichannel coupling effect was observed in the elastic ICS and DCSs. Although the comparison between the DCSs presented here and the DCSs reported in the literature is poor [15,17,18] (with the exception of the ones reported by Silva *et al.* [19]), the ICS agrees well with previous results [17,19]. Unfortunately, there are no experimental DCSs reported in the literature to date, which makes the analysis of the differences found in the calculated DCSs difficult. Furthermore, these results emphasize the importance of calculating the DCSs in addition to the ICS since it is a more detailed description of the scattering process.

The DCSs and ICS for the excitation from the ground state to the first four low-lying electronically excited states of formamide, namely, $1^3A'$, $1^3A''$, $1^1A''$, and $2^3A''$, were also reported. Once again, the multichannel coupling effect was observed. The comparison with the results from the literature [15,18] is poor due to pseudoresonances that appear in the electronically inelastic ICSs for energies below 20 eV. The partial ionization cross sections and TICS calculated with the BEB method and the TCS calculated as the sum of the elastic ICS, all electronically inelastic ICSs, and the TICS were also reported.

These calculations complement the previous work done with the SMCPP method [14,19,20], increasing the impact energies up to 50 eV and including electronic excitation channels. Although the investigation reported here enriches the

set of cross sections needed to develop precise mathematical models for interstellar and biological environments, further experimental work is needed to scrutinize the different calculations, especially regarding the DCSs.

[1] L. Sanche, Nature (London) **461**, 358 (2009).

[2] M. A. Huels, I. Hahndorf, E. Illenberger, and L. Sanche, J. Chem. Phys. **108**, 1309 (1998).

[3] B. Boudaïffa, P. Cloutier, D. Hunting, M. A. Huels, and L. Sanche, Science **287**, 1658 (2000).

[4] M. C. Boyer, N. Rivas, A. A. Tran, C. A. Verish, and C. R. Arumainayagam, Surf. Sci. **652**, 26 (2016).

[5] S. Pilling, D. P. P. Andrade, A. C. Neto, R. Rittner, and A. N. de Brito, J. Phys. Chem. A **113**, 11161 (2009).

[6] B. M. Bode and M. S. Gordon, J. Mol. Graphics Modell. **16**, 133 (1998).

[7] P. Cloutier, C. Sicard-Roselli, E. Escher, and L. Sanche, J. Phys. Chem. B **111**, 1620 (2007).

[8] R. H. Rubin, G. W. Swenson, Jr., R. C. Benson, H. L. Tigelaar, and W. H. Flygare, Astrophys. J. **169**, L39 (1971).

[9] J. M. Hollis, F. J. Lovas, A. J. Remijan, P. R. Jewell, V. V. Ilyushin, and I. Kleiner, Astrophys. J. **643**, L25 (2006).

[10] Y. A. Jeilani, H. T. Nguyen, D. Newallo, J.-M. D. Dimandja, and M. T. Nguyen, Phys. Chem. Chem. Phys. **15**, 21084 (2013).

[11] M. Seydou, A. Modelli, B. Lucas, K. Konate, C. Desfrancois, and J. P. Schermann, Eur. Phys. J. D **35**, 199 (2005).

[12] T. Hamann, A. Edtbauer, F. F. da Silva, S. Denifl, P. Scheier, and P. Swiderek, Phys. Chem. Chem. Phys. **13**, 12305 (2011).

[13] Z. Li, M. Ryszka, M. M. Dawley, I. Carmichael, K. B. Bravaya, and S. Ptasińska, Phys. Rev. Lett. **122**, 073002 (2019).

[14] M. H. F. Bettega, Phys. Rev. A **81**, 062717 (2010).

[15] Y.-F. Wang and S. X. Tian, Phys. Rev. A **85**, 012706 (2012).

[16] D. Gupta, R. Naghma, and B. Antony, Mol. Phys. **112**, 1201 (2014).

[17] M. G. P. Homem, I. Iga, G. L. C. de Souza, A. I. Zanelato, L. E. Machado, J. R. Ferraz, A. S. dos Santos, L. M. Brescanin, R. R. Lucchese, and M.-T. Lee, Phys. Rev. A **90**, 062704 (2014).

[18] M. Vinodkumar, C. Limbachiya, H. Desai, and P. C. Vinodkumar, J. Appl. Phys. **116**, 124702 (2014).

[19] M. O. Silva, G. M. Moreira, M. H. F. Bettega, and S. d'A. Sanchez, J. Phys. Chem. A **124**, 6009 (2020).

[20] M. O. Silva, G. M. Moreira, M. H. F. Bettega, and S. d'A. Sanchez, Chem. Phys. **555**, 111432 (2022).

[21] T. P. M. Goumans, F. A. Gianturco, F. Sebastianelli, I. Baccarelli, and J. L. Rivail, J. Chem. Theory Comput. **5**, 217 (2009).

[22] G. A. Gallup, J. Chem. Phys. **139**, 104308 (2013).

[23] R. F. da Costa, F. J. da Paixão, and M. A. P. Lima, J. Phys. B **38**, 4363 (2005).

[24] K. Takatsuka and V. McKoy, Phys. Rev. A **24**, 2473 (1981); Phys. Rev. A **30**, 1734 (1984).

[25] R. F. da Costa, M. T. do N. Varella, M. H. F. Bettega, and M. A. P. Lima, Eur. Phys. J. D **69**, 159 (2015).

[26] M. H. F. Bettega, L. G. Ferreira, and M. A. P. Lima, Phys. Rev. A **47**, 1111 (1993).

[27] G. B. Bachelet, D. R. Hamann, and M. Schlüter, Phys. Rev. B **26**, 4199 (1982).

[28] G. M. J. Barca *et al.*, J. Chem. Phys. **152**, 154102 (2020).

[29] M. H. F. Bettega, A. P. P. Natalense, M. A. P. Lima, and L. G. Ferreira, Int. J. Quantum Chem. **60**, 821 (1996).

[30] T. H. Dunning, Jr., J. Chem. Phys. **53**, 2823 (1970).

[31] W. J. Hunt and W. A. Goddard, III, Chem. Phys. Lett. **3**, 414 (1969).

[32] K. Emrich, Nucl. Phys. A **351**, 379 (1981).

[33] H. Sekino and R. J. Bartlett, Int. J. Quantum Chem. **26**, 255 (1984).

[34] J. F. Stanton and R. J. Bartlett, J. Chem. Phys. **98**, 7029 (1993).

[35] R. J. Bartlett, Wiley Interdiscip. Rev.: Comput. Mol. Sci. **2**, 126 (2012).

[36] D. G. A. Smith *et al.*, J. Chem. Phys. **152**, 184108 (2020).

[37] D. P. Chong, J. Electron Spectrosc. Relat. Phenom. **184**, 164 (2011).

[38] J. D. Hirst, D. M. Hirst, and C. L. Brooks, J. Phys. Chem. **100**, 13487 (1996).

[39] J. M. Gingell, N. J. Mason, H. Zhao, I. C. Walker, and M. R. F. Siggel, Chem. Phys. **220**, 191 (1997).

[40] R. H. Staley, L. B. Harding, W. A. Goddard III, and J. L. Beauchamp, Chem. Phys. Lett. **36**, 589 (1975).

[41] H. Basch, M. B. Robin, and N. A. Kuebler, J. Chem. Phys. **47**, 1201 (1967).

[42] Z. Benková, I. Cernusák, and P. Zahradník, Int. J. Quantum Chem. **107**, 2133 (2007).

[43] R. F. da Costa, M. T. do N. Varella, M. H. F. Bettega, R. F. Neves, M. C. A. Lopes, F. Blanco, G. García, D. B. Jones, M. J. Brunger, and M. A. P. Lima, J. Chem. Phys. **144**, 124310 (2016).

[44] R. D. Nelson, Jr., D. R. Lide, Jr., and A. A. Maryott, *Selected Values of Electric Dipole Moments for Molecules in the Gas Phase*, National Standard Reference Data System (Institute for Basic Standards, National Bureau of Standards, Washington, DC, 1967).

[45] Y. K. Kim and M. E. Rudd, Phys. Rev. A **50**, 3954 (1994).

[46] D. H. A. ter Steege, C. Lagrost, W. J. Buma, D. A. Leigh, and F. Zerbetto, J. Chem. Phys. **117**, 8270 (2002).

[47] H. Siegbarn, L. Asplund, P. Kelfve, K. Hamrin, L. Karlsson, and K. Siegbahn, J. Electron Spectrosc. Relat. Phenom. **5**, 1059 (1974)

[48] R. F. da Costa, M. H. F. Bettega, M. T. do N. Varella, E. M. de Oliveira, and M. A. P. Lima, Phys. Rev. A **90**, 052707 (2014).